JPhys Energy

PAPER • OPEN ACCESS

Performance and application of Si/$Ti_3C_2T_x$ (MXene) composites in lithium ion battery

To cite this article: Tingting Jiang *et al* 2023 *J. Phys. Energy* **5** 014020

View the article online for updates and enhancements.

You may also like

- In Situ Reduction of Gold Nanoparticle-Decorated Ti_3C_2 MXene for Ultrasensitive Electrochemical Detection of MicroRNA-21 with a Cascaded Signal Amplification Strategy
Xiao Yang, Linlin Zhao, Lin Lu et al.

- Review—$MoSe_2$ Nanostructures and Related Electrodes for Advanced Supercapacitor Developments
Rinky Sha, Palash Chandra Maity, Umamaheswari Rajaji et al.

- Harnessing the unique properties of MXenes for advanced rechargeable batteries
Deobrat Singh, Vivekanand Shukla, Nabil Khossossi et al.

This content was downloaded from IP address 80.2.41.206 on 13/02/2023 at 10:06

Journal of Physics: Energy

PAPER

Performance and application of $Si/Ti_3C_2T_x$ (MXene) composites in lithium ion battery

Tingting Jiang[1,*], **Qilun Xiong**[1], **Hao Yang**[1] and **George Z Chen**[2,*]

[1] The State Key Laboratory of Refractories and Metallurgy, College of Materials and Metallurgy, Wuhan University of Science and Technology, Wuhan 430081, People's Republic of China
[2] Department of Chemical and Environmental Engineering, Faculty of Engineering, University of Nottingham, Nottingham NG2 7RD, United Kingdom
* Author to whom any correspondence should be addressed.

E-mail: george.chen@nottingham.ac.uk

Keywords: performance, applications, Si/Ti_3C_2, MXene, composites, lithiums

OPEN ACCESS

RECEIVED
30 July 2022

REVISED
18 January 2023

ACCEPTED FOR PUBLICATION
27 January 2023

PUBLISHED
7 February 2023

Original content from this work may be used under the terms of the Creative Commons Attribution 4.0 licence.

Any further distribution of this work must maintain attribution to the author(s) and the title of the work, journal citation and DOI.

Abstract

The excellent theoretical specific charge (lithium) storage capacity and rich abundance of silicon (Si), and the good mechanical and electrical properties of titanium based MXene ($Ti_3C_2T_x$) nanosheets promise high performance composites ($Si/Ti_3C_2T_x$) for negative electrodes (negatrodes) in future lithium ion battery (LIB) applications. In particular, the $Si/Ti_3C_2T_x$ composites have been preliminarily shown to offer large and stable cyclic capacity, good rate capability and a highly profitable market prospect. To better understand and help further improve the electrochemical performance of these composites, this review focuses on the electrochemical processes occurring in Si/MXene composites from a material perspective. Different cells used for electrochemical measurements, the related materials properties and the reaction processes and kinetics of Si/MXene composites as negatrode in LIB are reviewed. The perspective is also discussed for practical applications in flexible electronic devices and automobiles.

1. Introduction

Facing numerous challenges including resource depletion and environmental disruption, fossil fuels and related technologies are being gradually replaced by those green and renewable ones. Wind and solar energy have been developed quickly in recent years, due to their inexhaustibility, affordability, and environmental benefits. However, the intermittence, instability, and geographic restriction in power output limit the large-scale application of renewable energy, unless necessary supporting technologies become available, particularly those capable of energy storage. Electrochemical energy storage (EES) devices, which have been utilized in portable electronic devices and electrical vehicles for years, are now being applied to store electricity generated by photovoltaic and wind power. As a typical EES device, lithium-ion battery (LIB) presents high voltage and energy density, and also satisfactory power capability and fairly long cycle life. To meet the ever-increasing demand in performance, cost, and safety, novel electrode materials have been investigated to achieve higher energy densities and longer cycle life [1, 2].

Silicon (Si) has been considered the most promising negative electrode (negatrode) material due to its ultra-high theoretical specific capacity for lithium (Li) storage (2112 mAh g^{-1} counting on the total mass of both Si and Li according to the negatrode reaction, $Si + nLi^+ + ne \rightleftharpoons SiLi_n$, $n \leqslant 4.4$) [3], appropriate electrode potentials, abundant resources, and being eco-friendly. However, disadvantages of Si limit its large scale and real application as negatrodes in LIBs, including low electric conductivity, large volume change during the Li storage process, unstable solid electrolyte interphase (SEI) film, and the resulting disconnection to the current collector, which have already arisen much attention of researchers [4–7].

Based on the related results of testing Si-based negatrode materials in half and full cells, the effective strategies can be summarized in two main aspects. The first is to construct nanomaterials with higher specific surface areas to maintain the structural integrity of Si during charge and discharge, and to improve the contacting area with electrolyte to achieve more effective carrier transportation. For example, Si

© 2023 Author(s). Published by IOP Publishing Ltd

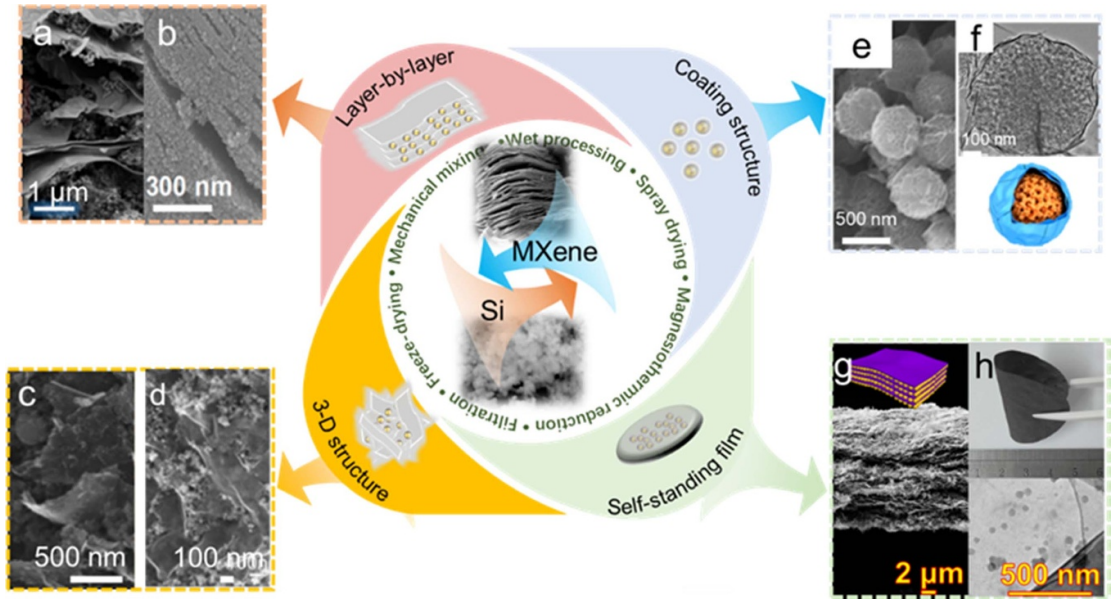

Figure 1. Schematic summary of the design and preparation of differently structured Si/MXene composites. (a) Side- and (b) cross-section SEM images of the Si/MXene composite with layer-by-layer structure. Adapted from [38]. CC BY 4.0., Adapted with permission from [39] Copyright (2019) American Chemical Society. (c), (d) SEM images of Si/MXene composites with 3D structure. Adapted with permission from [50], Copyright (2020) American Chemical Society., Adapted from [44], Copyright (2022), with permission from Elsevier. (e) SEM and (f) TEM images of Si/MXene composites with coating structure with a schematic overview in the inset. Adapted with permission from [36]. Copyright (2020) American Chemical Society. (g) Cross-sectional SEM image and (h) TEM images of self-standing films of Si/MXene composites. The insets are schematic illustration and photograph. Adapted with permission from [51], Copyright (2019) American Chemical Society.

nanoparticles (SiNPs), nanowires, nanotubes, hollow nanostructures, and porous structures have been proven to enhance the performances of Si-based negatrodes to different extents [8–11]. Secondly, compositing with other materials such as carbon [12–17], metal [18–20], and metal oxides [21, 22] could combine the advantages of both Si and other materials into the negatrode with larger capacity, longer cycle life, and higher stability. For example, the famous two-dimensional (2D) material, graphene, has been utilized as a buffer layer and conducting layer in Si-based composites due to its favorable flexibility, strength, and conductivity, which could help stabilize the integrity of Si and also assist the conduction of electron and Li^+ ion [15, 23–26].

As a rising star in 2D materials, especially for energy storage applications, MXene, the transition metal carbides/nitrides derived from dozens of MAX phase materials (M: transition metal element, A: an A group element, e.g. Al or Zn, X: C or N) has attracted much attention for alkaline metal ion batteries or supercapacitors [27–32]. Due to the remarkable electronic conductivity, good stability and flexibility, and tailorable surface functionality, MXene (in the following text, MXene represents the $Ti_3C_2T_x$ family unless specifically indicated) can be used to construct various composite structures with Si to obtain negatrode materials with excellent overall performance based on the synergistic effect of MXene and Si [33].

Like composites with other 2D materials, the structures of Si/MXene composites can be summarized into the four types: layer-by-layer assemblies, 3D structures, self-standing films, and coating structures (MXene coated on Si), which can be prepared in several ways, including mechanical mixing, wet processing, spray drying, magnesiothermic reduction, filtration, and freeze-drying [33]. A schematic summary of different preparation methods and structural features of Si/MXene composites can be seen in figure 1. Generally, the free-standing film and the coating structure can be prepared mainly from few-layer MXene nanosheets, while the layer-by-layer structure and 3D structure composites can be prepared with both few- and multi-layer MXenes.

In the layer-by-layer structure, SiNPs were anchored at the interlayer space of MXene layers, where the loose structure or interlayer structure could accommodate the large volume expansion of Si, helping maintain the stability of the whole composite structure, and providing the extra pathway for electrons and Li^+ ions [25, 34–38]. Both multi- and few-layer MXene could form a layer-by-layer structure with SiNPs. In the former case, SiNPs could decorate between the layers of MXene by mechanical mixing. In the latter case, MXene nanosheets could pile up with Si inside the interlayer spaces. A large specific surface area and loose structure could increase the contact between active material and electrolyte, but they may also lead to a low volumetric capacity. This structure can be achieved by several facile methods, such as wet processing and

mechanical mixing [37, 39–42]. In the wet-processing method, by dispersing the powders of Si, MXenes, and other components in the same solvent, a uniform solution/slurry can be formed, which leads to efficient mixing and self-assembly.

3D structures with thin multi-layer or few-layer MXene nanosheets derived from powdery multi-layer precursors as a skeleton can be fabricated via wet-processing (e.g. fluoride assisted exfoliation), freeze-drying, mechanical mixing, and magnesiothermic reduction. The obtained 3D porous structure could buffer the volume change of SiNPs during the charge and discharge processes, and also provide conductive pathways to ions and more active reaction sites [43–50].

As the most common composite structure, the coating structure can be obtained by several simple methods. The coating of few-layer MXenes on SiNPs can separate SiNPs from the electrolyte to obtain a more stable SEI film and prevent the pulverization and contact loss from the current collector of the Si negatrode. The surface control should be noticed to avoid aggregation to the greatest extent [36, 52–56].

Through filtration of the precursor, a self-standing film, in which few-layer MXene sheets act as the matrix of the thin film and embed SiNPs inside, with an interconnection can be prepared [45, 51, 57–60]. This integrated and independent film can be used directly in the half or full cell without the extra procedure of slurry preparation and coating on a copper (Cu) foil, which therefore eliminates the influence of binders and increase the weight ratio of active/supporting materials in the cell. What should be considered is that large-scale production needs to be designed carefully.

Previous research has shown that combining high-capacity Si with conductive and flexible MXene into a composite promises notably improved negatrode performances in LIB applications [37, 61]. However, factors affecting the electrochemical characteristics of Si/MXene composites have not been systematically studied, including the investigation medium and method, the mechanism of electrochemical reaction during the Li storage process. Also, the kinetics of electrode reactions have not always been explained directly and clearly. Therefore, in this review, the electrochemical performances, the measurement devices, and kinetic behavior of the Si/MXene composites as the negatrode material in LIB will be analyzed and discussed. The prospect of real applications will also be considered.

2. Cell setup

The design and construction of the evaluation cells for the electrode materials are of great significance, especially for novel electrode and electrolyte materials in all EES devices. Based on proper investigations of composite electrode materials, one can achieve a deeper understanding of the electrochemical mechanism during the energy storage process and prospect further development and application of new materials [62]. For negatrode materials, they should have a large theoretical capacity, sufficiently negative potential for Li^+ ion insertion, good chemical and mechanical stability, low or zero toxicity, and affordable cost.

To investigate novel composite negatrodes and the effective approaches to improving their performance relating to the structural design, a series of characterization methods should be applied to reveal the chemical state, crystal structure, and microstructure of the material. Such analytical findings can provide complementary information to understand the electrochemical testing results.

Electrochemical performances are usually studied by cyclic voltammetry (CV), galvanostatic charge–discharge (GCD), and electrochemical impedance spectroscopy (EIS), although other techniques such as galvanostatic intermittent titration can also help. The core of such measurements is the electrochemical cell whose setup and building materials may influence the testing process and results [63].

The most commonly used cells in laboratory include the coin type half cell and full cell, and the pouch or soft package type two-electrode full cell [62, 64]. In principle, the main difference between these cells is that the half cell can achieve the control and observation of the potential of the working electrode of the active material(s), but the full cell cannot. This is because in the half cell, the Li metal disc functions as both the reference and counter electrodes, which in a conventional electrochemical cell are two separate electrodes. However, the separation of the reference and counter electrodes is only necessary if the current passing through the combined reference-counter electrode causes polarization. Fortunately, when using a Li metal disc with a sufficiently large area in contacting with the electrolyte, polarization is usually small because the current density in the half cell is usually at or smaller than 1 mA cm^{-2}. In line with this understanding, the coin half cell for testing LIB electrode materials is equivalent to the conventional three electrode cell. In fact, the conventional three electrode cell is also known as a half cell because it can test the reaction on one of the two electrodes or in one of the two half cells of a full cell.

It is worth noting that the coin or pouch type two-electrode cells are usually asymmetrical with the two electrodes made from different materials. However, the two-electrode cell can also be symmetrical, i.e. the two electrodes are made from the same material, offering unique conditions for performance exploration.

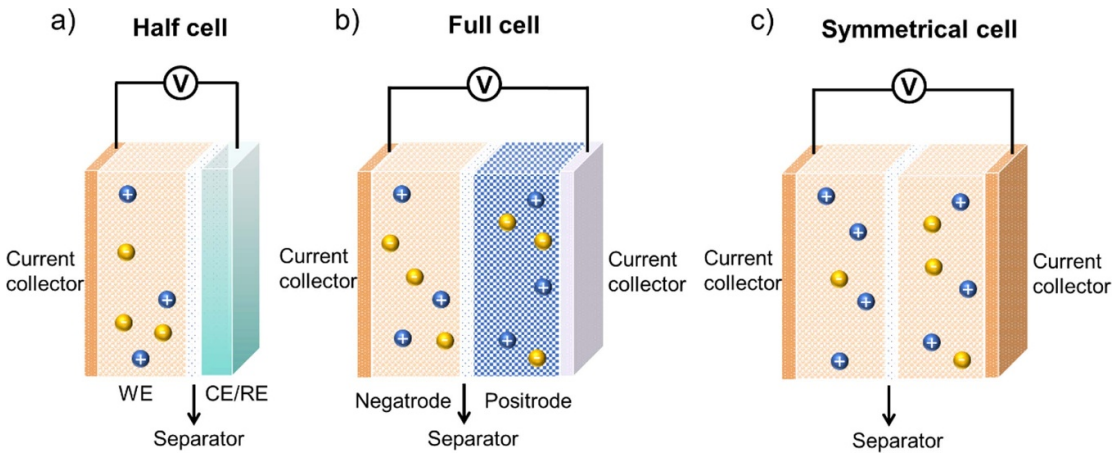

Figure 2. Types of cell setup for novel electrode materials investigation. (a) The half cell with the working electrode (WE) and a Li metal foil serving as both the counter electrode (CE) and reference electrode (RE), (b) the full-cell with negatrode and positrode, (c) the symmetrical cell consisting of two electrodes of the same material. Adapted from [64]. CC BY 4.0. © 2021 The Authors. Batteries & Supercaps published by Wiley-VCH GmbH.

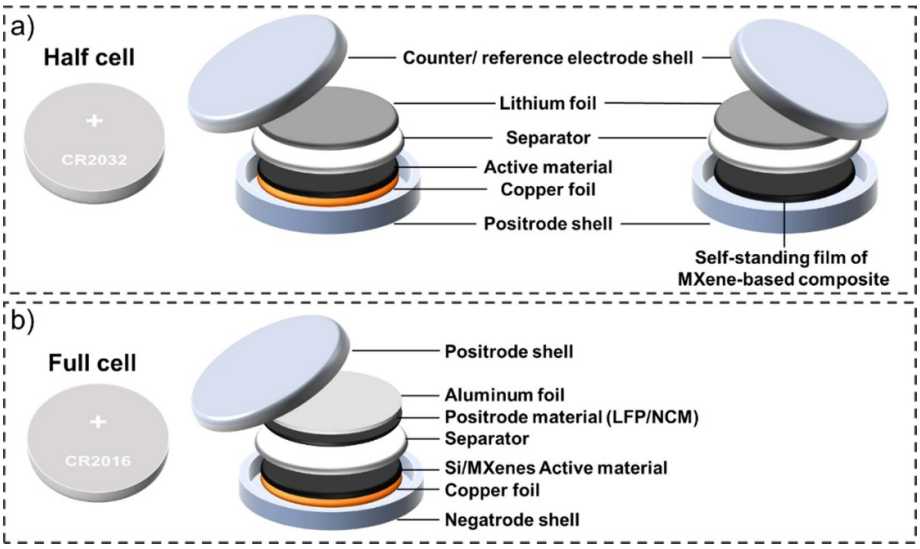

Figure 3. Expanded diagrams of coin type cells. (a) Half cells with copper as the current collector (left) and the self-standing film as the active negatrode (right), in which Li foil works as both the reference and counter electrodes, and (b) full cell containing both positrode and negatrode.

Figure 2 illustrates the working principles of these cells, whilst figure 3 explains the configurations of different coin type cells.

2.1. Half cell

The coin type half cell is mostly used in investigations of novel electrode materials, in which a Li-metal disc is used as both the counter electrode and reference electrodes. Such a half cell is easy to assemble on the specific equipment, commonly reliable, and can provide direct information on reactions on the prepared novel electrode. The schematic diagram of this type of cell can be seen in figure 2(a) [63]. In this half cell, for systematic research, the electrode material of interest is set as the working electrode to evaluate the potential-current-time correlations, and reversible storage characteristics.

While operating at a low-enough current density (considering the electrode surface area), the accuracy in the potential of the working electrode can be ensured, due to the negligible polarization at the counter/reference electrode (Li metal). Besides, the use of Li metal as the counter and reference electrode in the half cell can provide an infinite number of Li ions, which can help focus on the new electrode study. For a better understanding and clearer interpretation, the explicit term 'potential vs. Li/Li^+' should be used when reporting on this half cell, meaning the potential of the working electrode is determined with the help of the Li metal counter–reference electrode.

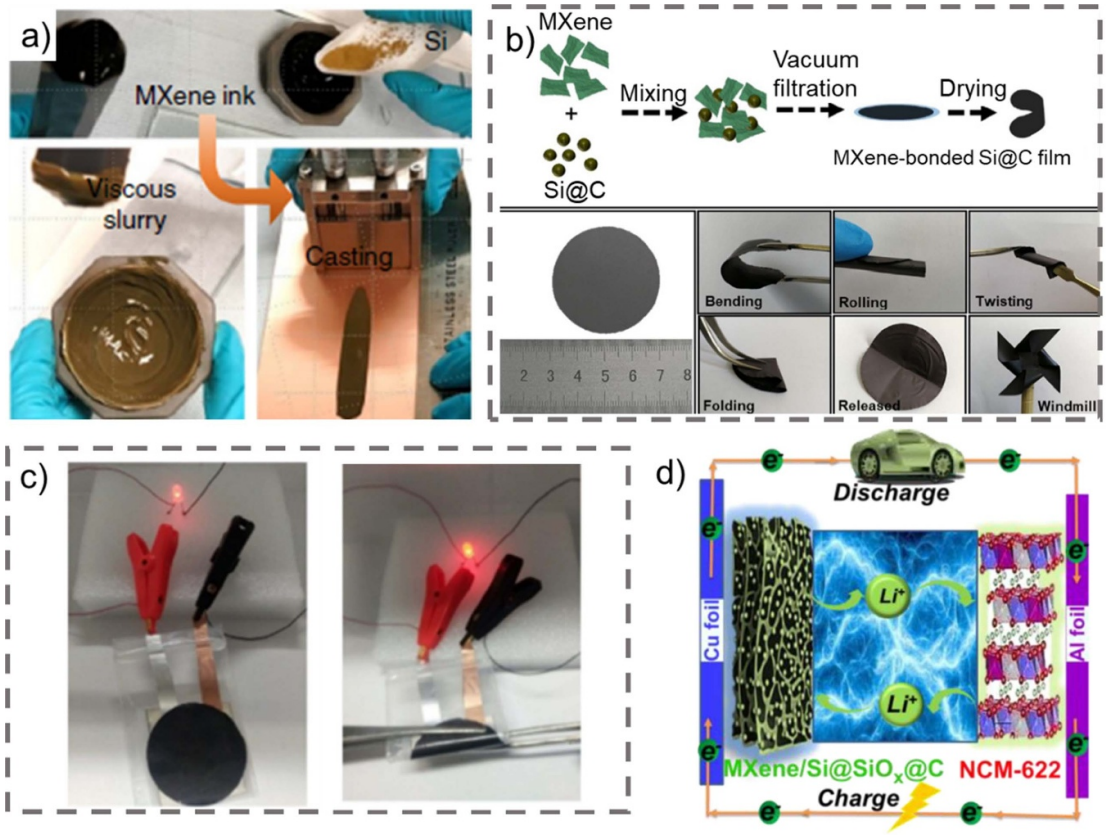

Figure 4. (a) Photographs showing the fabrication of the Si/MXene composite electrode by the ink-based slurry casting method. Adapted from [38]. CC BY 4.0. (b) Schematic illustration of the fabrication process of the self-standing Si/MXene film whose appearance and flexibility under different mechanical effects are shown in the photographs. Adapted from [60] John Wiley & Sons. © 2019 Wiley-VCH Verlag GmbH & Co. KGaA, Weinheim. (c) Photographs of the commercial red LED lit up by the pouch cells based on the Si/MXene composite self-standing film negatrode tested under the flat and bending states. Adapted from [45], with permission from Springer Nature. (d) Schematic illustration of the configuration of a full cell of MXene/Si@SiO_x@C || $Li[Ni_{0.6}Co_{0.2}Mn_{0.2}]O_2$. Adapted with permission from [39]. Copyright (2019) American Chemical Society.

In the development of Si/MXene composite negatrode materials, the half cell is also the most used investigation cell setup. There are two types of working electrodes, the slurry-type and the self-standing film.

Similar to the commercial LIB manufacturing process, the active material (Si/MXene composites) was mixed with the conducting agent (acetylene black, i.e. Super P), and polymeric binder (carboxymethyl cellulose, sodium alginate, polyvinylidene fluoride, polyacrylic acid) in a weight ratio of 6:2:2, or 8:1:1, for example. The mixture was dissolved or dispersed in deionized water (or other solvents) to form a homogenous slurry and spread onto the Cu foil. Then the electrode was dried under vacuum and pressed in air at 10 MPa.

In laboratory, the coin cell is often utilized as the half cell as mentioned above. In a typical example [63], the coin half cells (e.g. CR2032/2025/2016-type, see figure 1) were assembled in an argon-filled glovebox, where the prepared working electrode, polypropylene film as the separator, and Li foil were placed into the shell respectively. After that, the electrolyte with 1 M $LiPF_6$ in organic solvents (often a mixture of ethylene carbonate (EC) and dimethyl carbonate (DMC) (v/v = 1:1)) containing functional additives (i.e. 5% fluoroethylene carbonate (FEC)) was injected into the cell. A schematic assembling diagram can be seen in figure 3(a). The mass loading can be modified between 0.5–2 mg cm^{-2} (usually around 1 mg cm^{-2}). In some cases, the loaded mass can be up to 4 mg cm^{-2} by the use of a carbon-coated Cu foil [65].

Due to the unique nature of MXene, it is possible to prepare the Si/MXene viscous aqueous ink without any binder and other conductive additives, which can be spread directly on the current collector by a slurry-casting method [60]. The picture of a viscous ink and the casting process can be found in figure 4(a). Thus, the MXene nanosheets can form a continuous conductive network with the Si nanoparticles embedded in the network, resulting in fast charge transportation, strong mechanical stability, and effectively increased active materials content [38].

Another way to assemble a coin half cell is to use the Si/MXene self-standing film. After wet processing or other chemical reactions, the mixed colloidal solution of SiNPs and MXene nanosheets (single or few layers) was filtered through a membrane with the help of a vacuum. For example, a flexible and self-standing film of

Si@C/MXene was prepared by vacuum filtration of the mixture of Si@C and MXene, and the received film could afford various mechanical deformations such as bending, rolling, and twisting (figure 4(b)) [60], in which MXenes acted as not only the matrix fixing SiNPs but also the binder and conductive additive.

While assembling the half cell, the self-standing Si/MXene composite film could be cut into the designed size and shape, and put into the coin cell shell, instead of the Cu foil-loaded active material. Other setups including the Li metal counter and reference electrode, separator, and electrolyte can be the same as the slurry-type half cell, as shown in figure 3(b). The utilization of the self-standing film of Si/MXene composites could achieve a higher mass ratio of the active material, promising the possible application of LIBs in flexible devices as shown, for example, in figure 4(c) [45].

2.2. Full cell

Although the half cell with a Li metal counter-reference electrode is the mostly used characterization setup for investigation of novel electrode materials, several problems and limitations should be considered. For instance, to evaluate the long cycle life of the novel electrode, the half cell may undergo several hundred or more cycles. The long term stability of the Li metal electrode and its influence on the working electrode have been rarely considered and analyzed. Besides, while performing dis-/charging tests at a large specific current during rate performance characterization, the polarization at the Li metal electrode may not be negligible. Therefore, many researchers evaluated the electrochemical performance with the extra help of the full cell. As shown in figure 2(b), the full cell is consisting of the negatrode of interest and a commonly used or commercial positrode.

The full cell can be assembled in a coin type cell (i.e. CR2016) or a soft package type cell. Figure 3(c) shows the schematic diagram of the coin full cell. In current studies, $Li[Ni_{0.6}Co_{0.2}Mn_{0.2}]O_2$ (NCM622), $Li[Ni_{0.8}Co_{0.1}Mn_{0.1}]O_2$ (NCM811), $LiFePO_4$ (LFP), and $LiNi_{0.5}Mn_{0.5}O_4$ (LNMO) are commonly and widely utilized as the positrode material. An exemplar MXene/Si@SiO_x@C || $Li[Ni_{0.6}Co_{0.2}Mn_{0.2}]O_2$ full cell is shown in figure 4(d) [39]. This packaged or pouch full cell can provide a maximum value of specific energy of 485 Wh kg^{-1}, much larger than that of the state-of-the-art commercial LIBs (around 170 Wh kg^{-1}). Another Si/C@MXene || $LiFePO_4$ (LFP) full cell also demonstrated much higher specific energy around 400 Wh kg^{-1} than that of a Si/C || LFP full cell (76 Wh kg^{-1}) [36]. Different from the half cell, the electrode for the full cell should be pre-treated before assembling. Pre-lithiation, including powder pre-lithiation, electrochemical pre-lithiation, and chemical self-pre-lithiation, can be performed for better utilization of the Li resources and to improve the performance of Si/MXene composites in full cells.

In addition to the half cell and full cell (which usually consists of positrode and negatrode of different materials and hence is asymmetrical), the symmetrical cell as illustrated in figure 2(c) is another available setup, consisting of two identical or very similar electrodes, which are operated by controlling the cell voltage during the dis-/charge process. Till now, there is no report of Si/MXene composites investigated by the symmetrical cell [7].

3. Electrochemical properties

3.1. Li storage behavior of Si and MXene

In principle, the Li storage behavior of an Si/MXene composite is determined by both the Si and $Ti_3C_2T_x$ MXene. It is known that Si acts as negatrode material in LIBs via the alloy and de-alloy mechanism during dis-/charge, which faces the challenges of structural instability and poor Coulombic efficiency (CE).

Si is electrochemically lithiated via several binary phase transitions to several Li_xSi alloys according to the following reversible reactions:

$$\mathrm{Si} + (n+x)\,\mathrm{Li}^+ + (n+x)\,e^- \rightleftharpoons \mathrm{Li}_{n+x}\mathrm{Si} + n\mathrm{Li}^+ + ne^- \rightleftharpoons \mathrm{Li}_{n+x}\mathrm{Si}\ (n+x \leqslant 4.4)\,. \tag{1}$$

Note that the term 'Li_xSi alloys' is commonly used in the LIB literature, but these 'alloys' are actually stoichiometric compounds. At high temperatures (e.g. 415 °C), the lithiation process of Si was found by coulometric titration to include four stages at potentials of 332, 288, 158, 44, and 4 mV (vs. Li/Li^+), corresponding to the four transition phases of $Li_{12}Si_7$, $Li_{14}Si_6$, $Li_{13}Si_4$, and $Li_{22}Si_5$, respectively [8, 66]. The lithiation and delithiation curves of Si at 415 °C and room temperature can be seen in figure 5(a).

At room temperature, the galvanostatic potential profile of Si lithiation is fairly flat, and Si turned into $Li_{15}Si_4$ after the lithiation process [8, 68–74]. The metastable $Li_{15}Si_4$ phase was formed during a selective equilibrium process, in which further transformation to a new transition phase is hindered due to the unreachable activation energy at the low temperature. The variation in composition cannot lead to the structure transformation, resulting in a single phase with varying composition. Therefore, the $Li_{22}Si_5$ phase cannot be obtained at room temperature [75]. Upon reversing the current direction, the $Li_{15}Si_4$ phase was

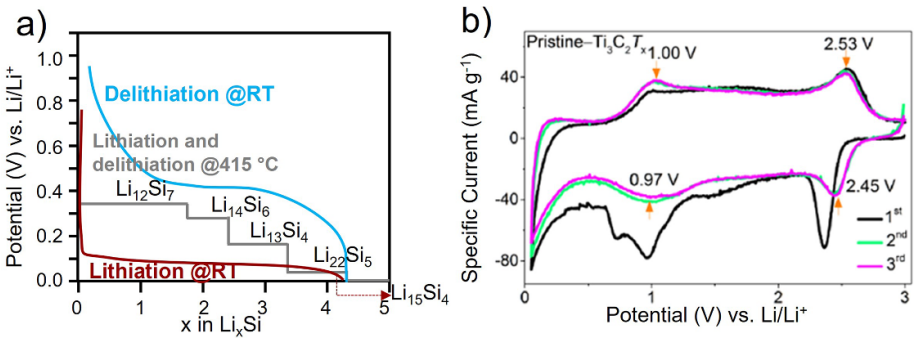

Figure 5. (a) Lithiation and delithiation of silicon at 415 °C (obtained by coulometric titration technique) and room temperature (schematic presentation according to experimental results). Adapted from [8], Copyright (2012), and adapted from [66]. Copyright (1981). With permission from Elsevier. (b) Three consecutive CVs of the pristine $Ti_3C_2T_x$. Adapted with permission from [67]. Copyright (2018) American Chemical Society.

delithiated and converted back to Si. Often, the potential plateaus at 0.1–0.2 V correspond to the alloying of Si. The electrochemical reaction process and the accompanying structural evolution of Si could guide the modification of Si negatrodes.

The interlayer space of $Ti_3C_2T_x$ MXenes is highly promising for lithiation properties, through the intercalation and deintercalation mechanisms with a potential range from 0.05 to 3.00 V vs. Li/Li^+. The related electrochemical reaction is shown below:

$$Ti_3C_2T_x + xLi^+ + xe^- \rightleftharpoons Li_xTi_3C_2T_x. \quad (2)$$

Figure 5(b) shows the initial three consecutive cyclic voltammograms (CVs) of pristine $Ti_3C_2T_x$ MXene at the scan rate of 0.1 mV s^{-1}. In all three cycles, two redox couples at 2.53 V/2.45 V and 1.00 V/0.97 V can be observed during the lithiation and delithiation process, respectively, which are similar to those reported in TiO_2 negatrode material. The obvious cathodic peak around 2.50 V and that between 0.80–1.00 V which became weaker in the subsequent two cycles indicate some irreversibility of the reactions of MXene in the first cycle. The good reproducibility and overlapping of the CVs in the second and third cycles indicate much improved reversibility and stability of the $Ti_3C_2T_x$ MXene negatrode for Li storage. As mentioned above, the tailored surface state with various surface functional groups of MXene could bring adjustable surface properties, which is closely related to the electrochemical performance. It should be noted that different Li-ion storage performances were observed in MXene materials upon different treatments and hence the reaction mechanisms [67].

3.2. Li storage reaction of Si/MXene composites

Compared to Si, the $Ti_3C_2T_x$ MXene can also provide a limited Li storage capacity at more positive potentials. In the Si/MXenes composite negatrode, Si acts as the main active material. However, to maximize the electrochemical performance and to better understand the mechanism of lithiation and delithiation of Si/MXenes composites, the potential range for the investigation is usually set as 0–3.00 V (2.50 V) vs. Li/Li^+.

The Si/MXene negatrode presents a similar electrochemical lithiation and delithiation behavior compared to a pure Si negatrode [34, 37, 51]. The broad reduction peak which appears around 0.8 V in the initial scan and is then absent in the subsequent cycles can be ascribed to the SEI layer formation on Si. Sometimes similar peaks at 1.00–1.40 V can be found, which are related to the irreversible reactions between surface functional groups of MXene and the electrolyte. The observed sharp cathodic peak near 0.10 V corresponds to the lithiation process of Si, where Si transforms into crystalline Li_xSi. Two oxidation peaks at approximately 0.30 V and 0.50 V may be due to the delithiation process, where Li_xSi turns back to the amorphous Si again. The redox peaks at 0.90 V and 1.1 V can be observed on some occasions, which are associated with Li intercalation and deintercalation in MXenes. Besides, the intensity of the current increases with the charge–discharge cycles, indicating an activation process of the composite, especially Si.

Figure 6(a) presents typical CVs of the Si/MXene composites in the potential range from 0 to 2.50 V, at a scanning rate of 0.1 mV s^{-1}, in the electrolyte of 1 M $LiPF_6$ in EC: DEC: ethyl 10 methyl carbonate (EMC) (1:1:1, in volume). Generally, compositing with MXene or adding carbon has little effect on the electrochemical reaction mechanism of the original Si. Figure 6(b) shows the CVs of Si and Si@MXene composite in a special electrolyte for Si negatrode purchased from *dodochem* in the initial cycle. On the one hand, the CVs in figures 5(b) and 6(a) show obvious capacitive features in addition to the current peaks, which should have resulted from the MXene matrix. On the other hand, the limited mass ratio of MXene/Si

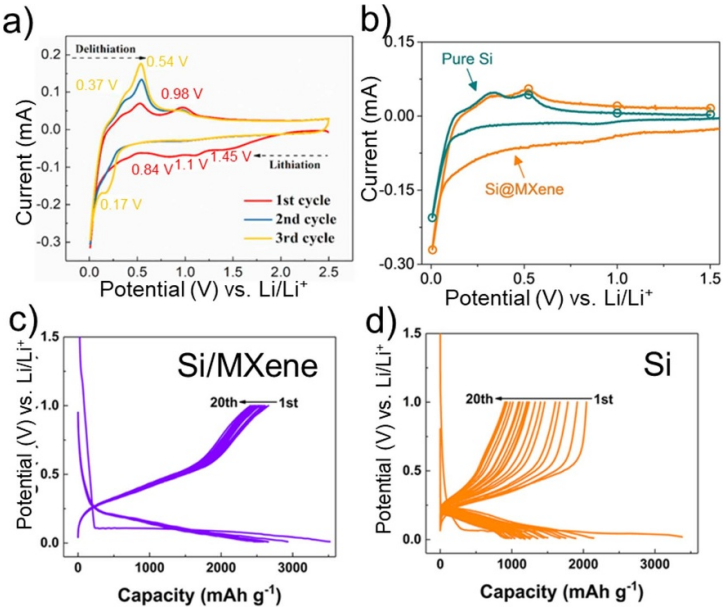

Figure 6. (a) CVs of the Si/MXene composite at 0.1 mV s^{-1} in the first three cycles (1 M LiPF6 in ethylene carbonate (EC): diethyl carbonate (DEC): ethyl 10 methyl carbonate (EMC) (1:1:1, in volume) as electrolyte, and at room temperature). Adapted from [37], Copyright (2018), with permission from Elsevier. (b) CVs of pure Si and Si@MXene of the initial cycle at a scan rate of 0.1 mV s^{-1} in the electrolyte suitable for silicon. (LX-025 from DodoChem) Adapted from [53] John Wiley & Sons. © 2021 Wiley-VCH GmbH. (c), (d) The first 20 GCD curves of Si/MXene (b) and Si (c) (the same electrolyte and temperature with (a)). Adapted with permission from [51]. Copyright (2019) American Chemical Society.

in the composites can provide an excellent framework in terms of transport of charge carriers. However, due to the well-modified structure, the natural stability and electroconductivity of MXene in comparison with the pure Si negatrode, the potential difference (ΔV) between the anodic and cathodic peaks on the CV of the Si/MXene composite negatrode is smaller, delivering a reduced polarization degree.

GCD is another most commonly used way to investigate the electrochemical performance of negatrode materials. Figures 6(b) and (c) present the first 20 GCD profiles of Si/MXene and pure Si, respectively. In both profiles, the potential plateaus of lithiation and delithiation are quite distinct in good agreement with the CVs. During the first charge, there was capacity loss in both samples, which can be ascribed to the SEI formation, the electrochemical decomposition of the electrolyte, and reactions between the electrolyte and surface groups of MXene. Compared to pure SiNPs, Si/MXene could deliver a higher capacity of around 2900 mAh g^{-1} after 20 cycles (figure 6(b)) and large initial CE (ICE) of 71%. The high reversibility of Si/MXene negatrodes was maintained after 100 cycles as a result of the more stable SEI layer and structure to hold Si nanomaterial inside, while the capacity of pure Si decayed fast. Therefore, MXene can effectively improve electrical conductivity, structural stability, and electrochemical reversibility.

3.3. Kinetic behavior of Si/MXene composites

EIS at open circuit potential (or voltage) can be conducted to verify the carrier transportation behavior in the novel negatrodes. The Nyquist plot of EIS (i.e. the complex plane plot of ac impedance) usually consists of a semicircle in the high-frequency region, which reflects the interfacial charge (electron or ion) transfer property, and an oblique straight line in the low-frequency region relating to the resistance and capacitance of the electrode material. As an example, the Nyquist plots of Si, MXene nanosheets, and Si@MXene as well as the equivalent circuit are presented in figure 7(a) [36]. The electrolyte was 1.0 M $LiPF_6$ in a mixture of EC, DMC, and ethyl methyl carbonate (EMC) (1:1:1 in volume).

The contact resistance (high frequencies) and charge transfer resistance (R_{ct}) of Si@MXene were found to be a little larger than those of the MXene nanosheets but much smaller than those of pure Si. This finding suggests that constructing the composite of Si with MXene can provide lower electronic resistance and faster Li^+ ion transport due to the structural features and good conductivity of MXene. According to the recorded Nyquist plots after a number of cycles, the charge transfer resistance of the Si/MXene composite always decreased as a result of the activation of the negatrode material, which is in accordance with the increased current density after activation from the CV investigation. Besides, the Li^+ ion diffusion coefficient D_{Li^+} can be calculated from the EIS results according to the following equation [44, 76]:

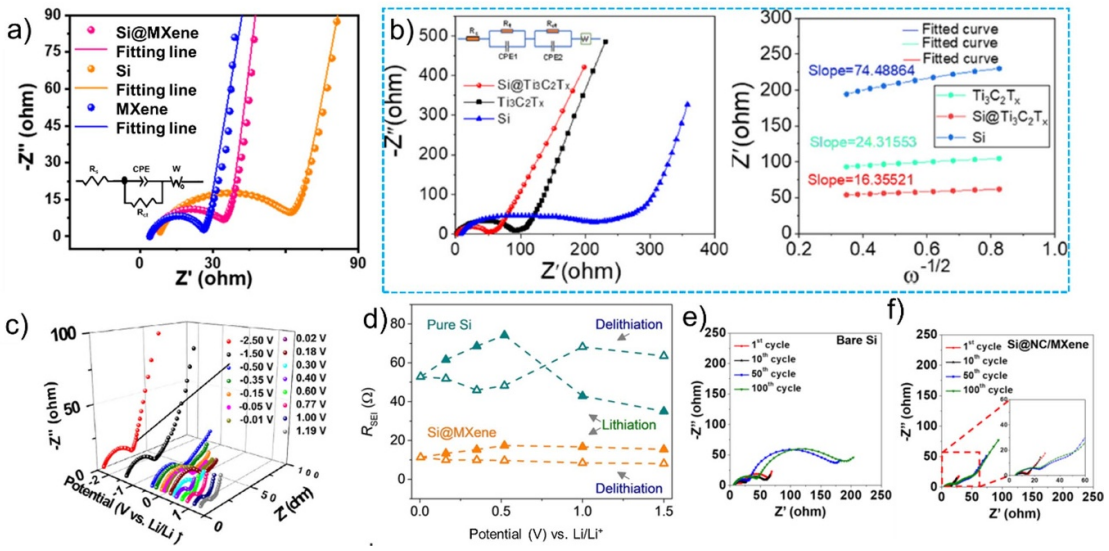

Figure 7. (a) EIS (Nyquist) plots and the related fitting curves of Si, MXene, and Si@MXene according to the equivalent circuit shown. Adapted with permission from [36]. Copyright (2020) American Chemical Society. (b) EIS plots (left), and the linear fitting of Z' vs. $\omega^{-1/2}$ (right) of Si, MXene, and Si@MXene. Adapted from [44], Copyright (2022), with permission from Elsevier. (c) EIS plots of Si@N-doped C/MXene at various potentials in the initial cycle. Adapted from [43], Copyright (2021), with permission from Elsevier. (d) Variation in SEI resistance at different potentials in the first cycle of pure Si and Si@MXene. Adapted from [53] John Wiley & Sons. © 2021 Wiley-VCH GmbH. EIS (Nyquist) plots of (e) silicon and (f) Si@NC/MXene at 1st, 10th, 80th, and 100th cycles. Adapted from [43], Copyright (2021), with permission from Elsevier.

$$D_{Li^+} = \frac{R^2T^2}{2A^2n^4F^4C^2\sigma^2} \tag{3}$$

where A is the surface area of the electrode, n the number of electrons attending the electronic transfer reaction, F the Faraday constant, C the concentration of Li^+ ion in the target negatrode, R the gas constant, T the temperature in the whole experiment, σ the Warburg coefficient which can be calculated from the linear fitting of Z' vs. $\omega^{-1/2}$. Figure 7(b) [44] shows the respective fitting curves calculated from the impedance spectra of Si, $Ti_3C_2T_x$ MXene, and Si@MXene in 1 M $LiPF_6$ dissolved in the 1:1 (v/v) mixture of EC/DEC. It can be seen that the values of the Warburg coefficient of the three electrodes were 74.5, 24.3, and 16.4, respectively. The Si@MXene sample was prepared by wet processing and freeze drying to form the 3D conductive network, which might have enabled a high specific capacity above 1700 mAh g^{-1} after 500 cycles at 1 A g^{-1}. The diffusion coefficients of Li^+ ion in Si, $Ti_3C_2T_x$ MXene, and Si@MXene negatrodes were derived from the Warburg coefficients as 0.4, 3.8, and 8.4 $\times$ 10^{-14} cm^2s^{-1}, respectively.

Apparently, Li-ion transportation was much faster in Si@MXene than in pure Si, suggesting the benefits of the structure design and synergistic effect of the composites in facilitating the electrochemical processes. The difference in EIS plots of pure Si in the medium frequency range in figures 7(a) and (b) may be caused by the difference in electrolyte, Si material and electrode fabrication. Apart from the difference in electrolyte solvents as mentioned above, the Si in figure 7(a) was porous spheres with a diameter of 400 nm prepared by magnesiothermic reduction from silica nanospheres, while the Si powders in figure 7(b) were purchased with a particle size less than 50 nm. Further, the Si electrodes were differently made, i.e. casting vs. doctor-blading. It seems that doctor-blading exerted an additional pressure and hence made a denser and more resistive coating than casting. Further, the manual operation of doctor-blading might have also led to less consistent samples than casting, which may be responsible for the unusual shape of the EIS plot of Si in figure 7(b).

Figure 7(c) [43] shows the Nyquist plots of the Si@N-doped C coupled with MXene nanosheets at various potentials listed on the right side. The electrolyte was 1 M $LiPF_6$ dissolved in a mixture of (EC/DEC; 1:1 v/v) with 5 wt% FEC. In the discharging process (the potential became less positive), the total resistance of the composites remained almost unchanged, while during the subsequent charging process (the potential became more positive), the total resistance of the composites decreased due to the dealloying effect. (Author note: the original paper has labeled potentials in figure 7(c) incorrectly with negative values in the discharging process).

The EIS investigation of pure Si and Si@MXene negatrodes was also performed and compared at different potentials [53]. The results are shown in figure 7(d), indicating that the SEI resistance of the composite was smaller and changed less during the lithiation and delithiation processes than that of the pure Si electrode, indicating formation of a more stable SEI layer in the composite with the help of 2D MXene nanosheets.

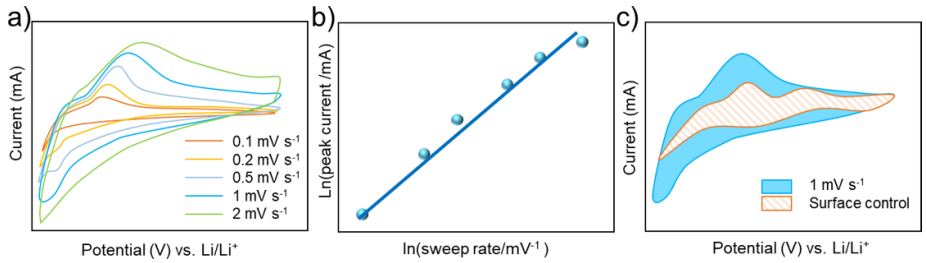

Figure 8. Illustration of (a) CVs of Si/MXene composites at different scan rates. (b) The linear fit of peak current vs. scan rate at the Napierian (natural) logarithm scale. (c) The CV recorded at a scan rate of 1 mV s^{-1} and the curve indicated by 'surface control' was calculated according to equation (5). Redrawn according to [23, 50, 61].

The related Si@MXene composite with a coating structure exhibited high capacity and good retention stability as high as 94% after 100 cycles. The EIS investigation proved this excellent performance again.

Figures 7(e) and (f) presented the Nyquist plots after several cycles of Si and a Si/carbon/MXene composite (Si@NC/MXene), respectively, which all fit well with the equivalent circuit model. The charge transfer resistance of pure Si increased as the cycling proceeded, indicating the pulverization of Si and the degraded stability. On the other hand, the plots of Si@NC/MXene exhibited a stable trend, indicating higher structural stability and robustness of the composite.

To further investigate the electrochemical processes, especially the reaction kinetics or ion transport dynamics of Si/MXene composites, CVs are usually recorded at different potential scan rates and analyzed [23, 45–47, 50, 58, 61, 65, 77, 78]. It has long been established in CV of a sufficiently thin coating capable of charge storage via either the electric double layer capacitance or a Faradaic mechanism, the current should be proportional to the potential scan rate. This behavior is known as a surface confined or controlled process.

However, when the coating become thicker, to maintain electric neutrality, the ingression including intercalation of the charge balancing counter ion will become diffusion controlled, leading to the current on the CV becoming proportional to the square root of the scan rate. It is also very common that for a given coating of an appropriate thickness, the current is proportional to the scan rate in a range of low scan rates, but becomes diffusion controlled at higher scan rates [79].

This understanding of either surface or diffusion control or both is applicable to any electrode with a coating that is capable of Li^+ ion storage [79]. The analysis of these two types of control can be obtained based on the relationship between the current (i) and the scan rate (v) linked by the following equations [31, 80–82]:

$$i = av^b \tag{4}$$

$$i = k_1 v + k_2 v^{1/2} \tag{5}$$

where a, b, k_1, and k_2 are parameters that can be determined experimentally. The value of b can be determined by the slope in the linear fitting of log$i$ vs. log$v$, which is associated with the Li^+ ion storage mechanism of the negatrode. The value of b is in the range of 0.5–1. Generally, $b = 0.5$ implies diffusion control, while $b = 1$ means surface control.

Figures 8(a) and (b) show the CVs at a series of scan rates and the linear fitting results, respectively. The shaded area in figure 8(c) was calculated according to the above equations. However, in some reports, the surface-controlled behavior is directly defined as the capacitive model, and the capacitive and diffusion-controlled Faradaic mechanisms are considered distinct from each other. Such an analysis and judgment are not appropriate, especially in the discussion of the Li storage mechanism. Generally, one can obtain the b value in Si-based electrodes for LIBs between 0.5 and 1, indicating the combined contribution of both diffusion-limited and surface-confined processes. However, in many literatures, the calculated surface-confined contribution increased surprisingly with the scan rate, which is opposite to expectation. Such a discrepancy may be accounted for as follows.

A zero or negligible ohmic drop of the electrode is the precondition to utilize equations (4) and (5) since the fitting was operated at the same potential. Otherwise, the current peak shift to the scanning direction can be observed on the CVs. For example, in figure 8(a), the oxidation peak has shifted obviously to more positive potentials. In such a case, the ohmic drop makes the actual electrode potential lower than the applied potential which is recorded on the CV. As a result, the measured CV current is also smaller than what would be expected in the absence of the ohmic drop. This ohmic drop effect is mathematically, for the same v, smaller on the $k_2 v^{1/2}$ term than the $k_1 v$ term in equation (5).

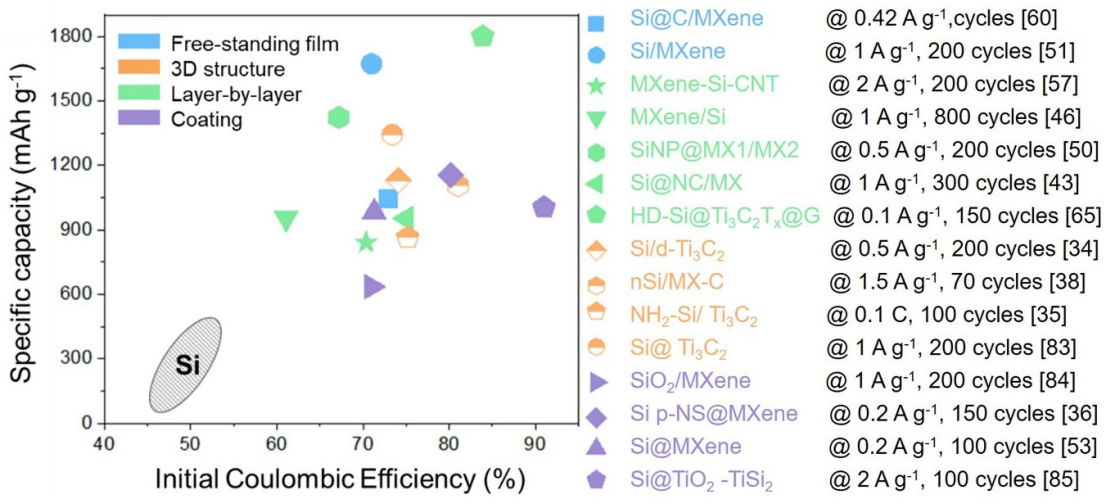

Figure 9. Collection of the specific capacity after dis-/charge cycling and ICE in recently reported advanced Si/MXene-based negatrodes. The above results are collected from the [34–36, 38, 43, 46, 50, 51, 53, 54, 57, 60, 65, 83–85].

Thus, when diffusion control is expected to increase at higher scan rates, the ohmic drop effect reduces the diffusion contribution to the measured CV current at the given fitting potential. This distortion should be particularly more serious at potentials before the current peak because diffusion becomes more influential at or after the peak potential. Therefore, for an electrode with a non-negligible ohmic resistance, part of the diffusion contribution is missing in the fitting results, leading to an apparently larger but misleading surface contribution.

It is worth noting that in a practical battery, diffusion control lowers the rate capability and should always be avoided. Therefore, equations (4) and (5) (and their derivatives) are very useful for analyzing electrode performance against the electrode material and structure to avoid the diffusion restriction during charging and discharging. Compared to pure Si, Si/MXene composites can provide better rate capability and cyclability due to the high conductivity of MXene and the constructed porous structure [77].

To further study the charge storage mechanism of Si/MXene, especially the synergy effect in the composites, *in situ* or *ex situ* spectroscopic and microscopic characterizations have been utilized during electrochemical investigations. For example, *ex situ* x-ray diffraction (XRD) analysis was performed by Zhang *et al* [39] to evaluate the interlayer spacing of MXene to figure out the volume buffering effect of the MXene matrix, indicating the promising elasticity and adjustability of MXene. Similar to the investigation on the lithiation process of pure Si, *in situ* TEM was also carried out on the Si/MXene composite to examine the whole de-/lithiation process [57, 65].

3.4. Charge storage performance of Si/MXene composites

As briefly described in the Introduction section, Si/MXene composites can be prepared via a series of methods and categorized into four kinds of structures. Based on the variation in preparation method and the structural design, composites may exhibit different electrochemical performances.

Generally, MXene is introduced to solve the problems in Si negatrode, including the pulverization and contact loss caused by large volume changes during charge and discharge, poor electrical conductivity and ion transportation characteristics, and the unstable and repeatedly formed SEI layer. As a novel 2D flexible and highly conductive material, MXene can be involved in composites in various forms.

Regardless of the specific structural design, MXene can buffer the large volume expansion during the lithiation process and ensure mechanical integrity and stability in both the coating and 3D framework structures. These merits should lead to a stable long cycle capacity of the Si/MXene composites. The high electronic conductivity of MXene can improve the electron transportation of the whole composite negatrode. Meanwhile, the loose structure introduced by MXene can provide more electrolyte channels and ion pathways.

Instead of the facile mechanical mixing, modifying the surface structure of SiNPs and MXene may enable the formation of a more stable bonding, which can prevent the exfoliation and aggregation of SiNPs. As a result, a more stable SEI layer can form due to the wrapped MXene layer, which should improve both the long cycle capacity and rate capability at a large current. The corresponding capacity after cycles and the ICE of various Si/MXene composites have been collected and compared in figure 9. Similar composite structures

are indicated by the same color. The grey shaded area represents the pure Si performance, showing fairly poor cyclic stability and reversible capacity after only dozens of cycles.

After compositing with MXene in various structures (sometimes also with other materials such as SiO_x or carbon), the ICE increased to 70%–90%, and the long cycle capacity (i.e. the capacity at the number of cycles after which Si would have failed) could be improved to around 1000 mAh g^{-1} or larger at 0.1 A g^{-1}, 1 A g^{-1} or even higher specific currents. The enhanced ICE and long cycle capacity can be attributed mainly to the composite structure of Si/MXene where the highly conductive MXene layer could act as a barrier to prevent the direct contact of Si with electrolyte, and therefore help stabilize the SEI layer and improve the long cycle performance.

4. Conclusion and prospective

Si-based composites have been regarded as the most promising negatrodes in the next generation LIBs for electric vehicles and energy storage plant applications. To improve the cycling stability and rate capability of Si by modification is the most important strategy. Compositing with the flexible and conductive MXene could provide various composite structures with controllable micro-morphology and surface state, resulting in the improved mechanical property and carrier transport efficiency.

The three-electrode cell or half cell with a novel Si/MXene composite as the working electrode and a Li foil as the reference and counter electrodes is the mostly used cell set up in the investigation of the electrochemical performances of Si/MXenes. Due to the special structures of MXene and Si/MXene composites, the negatrode can be prepared by the conventional slurry-type method which is similar to that in industrial production, but can directly be applied with the as-prepared self-standing films of Si/MXene composites. Full cells of Si/MXene have been fabricated with several positrodes and presented excellent energy densities. However, further and large-scale investigations of compatibility with the positrodes and the assembling process are still needed.

At present, various structures of Si/MXene composites have been achieved by different fabrication methods, showing a better Li storage performance due to several advantages. (a) The flexible MXene nanosheets can act as a buffer layer or framework in composite structures and prevent SiNPs from fracturing and falling from the current collector, resulting in a higher capacity retention. (b) The more effective electrolyte wetting in negatrode and majority transportation channels for Li^+ ion can be formed in the porous structure, which together with the good conductivity of MXene can bring about better rate performances. (c) Due to the fairly strong bonding between Si and MXene surface groups, SiNPs can be anchored strongly to the MXene nanosheets. Therefore, MXene can also be used as a binder in Si-based negatrodes instead of the conventional inactive binders like polyvinylidene fluoride (PVDF) or carboxymethyl cellulose (CMC), leading to a higher mass ratio of active materials and hence better electrochemical performance and stability.

From the view of the large-scale application in energy storage devices, there are some superiorities and issues to be considered. Firstly, Si/MXene composites, especially the self-standing composite film, exhibit superior flexibility, which is the promising candidate for negatrodes of flexible LIBs in wearable electronics or other extreme conditions. Secondly, in different fabrication methods, some routines are compatible with the recent industrial manufacturing process of negatrodes. Therefore, the large-scale and commercial use of Si/MXene composite negatrodes are possible and implementable in the future. Last but not the least, referring to the Si-based full cell, Si/MXene composites also have the strength to be compatible with other battery components and can be pre-lithiated by various processes and provide a stronger SEI layer with the help of MXene.

Data availability statement

No new data were created or analysed in this study.

Acknowledgments

This work was supported by Natural Science Foundation of Hubei Province (2021CFB434), and National Natural Science Foundation of China (No. 51602234).

Conflict of interest

The authors declare no conflict of interest.

ORCID iDs

Tingting Jiang https://orcid.org/0000-0002-6924-7613
George Z Chen https://orcid.org/0000-0002-5589-5767

References

[1] Wang F, Wu X, Li C, Zhu Y, Fu L, Wu Y and Liu X 2016 Nanostructured positive electrode materials for post-lithium ion batteries *Energy Environ. Sci.* **9** 3570–611
[2] Han G-B, Ryou M-H, Cho K Y, Lee Y M and Park J-K 2010 Effect of succinic anhydride as an electrolyte additive on electrochemical characteristics of silicon thin-film electrode *J. Power Sources* **195** 3709–14
[3] Jiang T, Xu X and Chen G Z 2020 Silicon prepared by electro-reduction in molten salts as new energy materials *J. Energy Chem.* **47** 46–61
[4] Li P, Kim H, Myung S-T and Sun Y-K 2021 Diverting exploration of silicon anode into practical way: a review focused on silicon-graphite composite for lithium ion batteries *Energy Storage Mater.* **35** 550–76
[5] Di F, Zhou W, Yang H, Sun C, Geng X, Chen Y, Li L, Liu Z and An B 2021 Surface modification and functional structure space design to improve the cycle stability of silicon based materials as anode of lithium ion batteries *Coatings* **11** 1047
[6] Azam M A, Safie N E, Ahmad A S, Yuza N A and Zulkifli N S A 2021 Recent advances of silicon, carbon composites and tin oxide as new anode materials for lithium-ion battery: a comprehensive review *J. Energy Storage* **33** 102096
[7] Guo J *et al* 2021 Silicon-based lithium ion battery systems: state-of-the-art from half and full cell viewpoint *Adv. Funct. Mater.* **31** 2102546
[8] Wu H and Cui Y 2012 Designing nanostructured Si anodes for high energy lithium ion batteries *Nano Today* **7** 414–29
[9] Szczech J R and Jin S 2011 Nanostructured silicon for high capacity lithium battery anodes *Energy Environ. Sci.* **4** 56–72
[10] Kim H, Lee E-J and Sun Y-K 2014 Recent advances in the Si-based nanocomposite materials as high capacity anode materials for lithium ion batteries *Mater. Today* **17** 285–97
[11] Su X, Wu Q, Li J, Xiao X, Lott A, Lu W, Sheldon B W and Wu J 2014 Silicon-based nanomaterials for lithium-ion batteries: a review *Adv. Energy Mater.* **4** 1300882
[12] Jiao M, Wang Y, Ye C, Wang C, Zhang W and Liang C 2020 High-capacity SiO_x ($0 \leqslant x \leqslant 2$) as promising anode materials for next-generation lithium-ion batteries *J. Alloys Compd.* **842** 155774
[13] You S, Tan H, Wei L and Tan W and Chao Li C 2021 Design strategies of Si/C composite anode for lithium-ion batteries *Chem. Eur. J.* **27** 12237–56
[14] Kowase T, Hori K, Hasegawa K, Momma T and Noda S 2017 A-few-second synthesis of silicon nanoparticles by gas-evaporation and their self-supporting electrodes based on carbon nanotube matrix for lithium secondary battery anodes *J. Power Sources* **363** 450–9
[15] Tang F, Jiang T, Tan Y, Xu X and Zhou Y 2021 Preparation and electrochemical performance of silicon@graphene aerogel composites for lithium-ion batteries *J. Alloys Compd.* **854** 157135
[16] Li P, Zhao G, Zheng X, Xu X, Yao C, Sun W and Dou S X 2018 Recent progress on silicon-based anode materials for practical lithium-ion battery applications *Energy Storage Mater.* **15** 422–46
[17] Shi Q, Zhou J, Ullah S, Yang X, Tokarska K, Trzebicka B, Ta H Q and Rümmeli M H 2021 A review of recent developments in Si/C composite materials for Li-ion batteries *Energy Storage Mater.* **34** 735–54
[18] Li J, Fa W, Zhao H, Zhu C, Jia H and Gu L 2019 Dendritic silver hierarchical structures for anode materials in Li ion batteries *Micro Nano Lett.* **14** 887–91
[19] Ohta R, Fukada K, Tashiro T, Dougakiuchi M and Kambara M 2018 Effect of PS-PVD production throughput on Si nanoparticles for negative electrode of lithium ion batteries *J. Phys. D: Appl. Phys.* **51** 105501
[20] Yoo S, Lee J-I, Ko S and Park S 2013 Highly dispersive and electrically conductive silver-coated Si anodes synthesized via a simple chemical reduction process *Nano Energy* **2** 1271–8
[21] Yang J *et al* 2017 Amorphous TiO_2 shells: a vital elastic buffering layer on silicon nanoparticles for high-performance and safe lithium storage *Adv. Mater.* **29** 1700523
[22] Li Y, Sun Y, Xu G, Lu Y, Zhang S, Xue L, Jur J S and Zhang X 2014 Tuning electrochemical performance of Si-based anodes for lithium-ion batteries by employing atomic layer deposition alumina coating *J. Mater. Chem.* **2** 11417–25
[23] Meng J, Zhang F, Zhang L, Liu L, Chen J, Yang B and Yan X 2020 Rolling up MXene sheets into scrolls to promote their anode performance in lithium-ion batteries *J. Energy Chem.* **46** 256–63
[24] Zhang F, Jia Z, Wang C, Feng A, Wang K, Hou T, Liu J, Zhang Y and Wu G 2020 Sandwich-like silicon/$Ti_3C_2T_x$ MXene composite by electrostatic self-assembly for high performance lithium ion battery *Energy* **195** 117047
[25] Han X, Zhang Z, Chen H, Zhang Q, Chen S and Yang Y 2020 On the interface design of Si and multilayer graphene for a high-performance Li-ion battery anode *ACS Appl. Mater. Interfaces* **12** 44840–9
[26] Yang Y, Yang H-X, Wu Y-Q, Pu H, Meng W-J, Gao R-Z and Zhao D-L 2020 Graphene caging core-shell Si@Cu nanoparticles anchored on graphene sheets for lithium-ion battery anode with enhanced reversible capacity and cyclic performance *Electrochim. Acta* **341** 136037
[27] Srimuk P, Kaasik F, Krüner B, Tolosa A, Fleischmann S, Jäckel N, Tekeli M C, Aslan M, Suss M E and Presser V 2016 MXene as a novel intercalation-type pseudocapacitive cathode and anode for capacitive deionization *J. Mater. Chem.* **4** 18265–71
[28] Wang Z, Xu Z, Huang H, Chu X, Xie Y, Xiong D, Yan C, Zhao H, Zhang H and Yang W 2020 Unraveling and regulating self-discharge behavior of $Ti_3C_2T_x$ MXene-based supercapacitors *ACS Nano* **14** 4916–24
[29] Naguib M, Kurtoglu M, Presser V, Lu J, Niu J, Heon M, Hultman L, Gogotsi Y and Barsoum M W 2011 Two-dimensional nanocrystals produced by exfoliation of Ti_3AlC_2 *Adv. Mater.* **23** 4248–53
[30] Luo J, Matios E, Wang H, Tao X and Li W 2020 Interfacial structure design of MXene-based nanomaterials for electrochemical energy storage and conversion *InfoMat* **2** 1057–76
[31] Huang H, Cui J, Liu G, Bi R and Zhang L 2019 Carbon-coated $MoSe_2$/MXene hybrid nanosheets for superior potassium storage *ACS Nano* **13** 3448–56
[32] Bashir T, Li X, Yang S, Song Y, Zhou S, Wang J, Zhu W, Yang J, Zhao J and Gao L 2022 Enhancing role of structurally integrated V_2C MXene nanosheets on silicon anode for lithium storage *J. Alloys Compd.* **922** 166213

[33] Jiang T, Yang H and Chen G Z 2022 Enhanced performance of silicon negative electrodes composited with titanium carbide based MXenes for lithium-ion batteries *Nanoenergy Adv.* **2** 165–96

[34] Zhu X, Shen J, Chen X, Li Y, Peng W, Zhang G, Zhang F and Fan X 2019 Enhanced cycling performance of Si-MXene nanohybrids as anode for high performance lithium ion batteries *Chem. Eng. J.* **378** 122212

[35] Cui Y, Wang J, Wang X, Qin J and Cao M 2020 A hybrid assembly of MXene with NH_2-Si nanoparticles boosting lithium storage performance *Chem. Asian J.* **15** 1376–83

[36] Xia M, Chen B, Gu F, Zu L, Xu M, Feng Y, Wang Z, Zhang H, Zhang C and Yang J 2020 $Ti_3C_2T_x$ MXene nanosheets as a robust and conductive tight on Si anodes significantly enhance electrochemical lithium storage performance *ACS Nano* **14** 5111–20

[37] Kong F, He X, Liu Q, Qi X, Sun D, Zheng Y, Wang R and Bai Y 2018 Enhanced reversible Li-ion storage in Si@Ti_3C_2 MXene nanocomposite *Electrochem. Commun.* **97** 16–21

[38] Zhang C J, Park S H, Seral-Ascaso A, Barwich S, McEvoy N, Boland C S, Coleman J N, Gogotsi Y and Nicolosi V 2019 High capacity silicon anodes enabled by MXene viscous aqueous ink *Nat. Commun.* **10** 849

[39] Zhang Y, Mu Z, Lai J, Chao Y, Yang Y, Zhou P, Li Y, Yang W, Xia Z and Guo S 2019 MXene/Si@SiO_x@C layer-by-layer superstructure with autoadjustable function for superior stable lithium storage *ACS Nano* **13** 2167–75

[40] Zheng M and Wu S 2022 A novel method for synthesizing $Ti_3C_2T_x$ MXene nanosheets supported Si nanoparticles as lithium-ion batteries anode for electric vehicles applications *Mater. Lett.* **311** 131570

[41] Liu X H, Zhong L, Huang S, Mao S X, Zhu T and Huang J Y 2012 Size-dependent fracture of silicon nanoparticles during lithiation *ACS Nano* **6** 1522–31

[42] Liu J, Song S, Zuo D, Yan C, He Z, Li Y and Zheng J 2020 Synthesis and characterization of SiO_2/Ti_3C_2 anode materials for lithium-ion batteries via different methods *Ionics* **26** 5325–31

[43] Jo D Y, Kim J K, Oh H G, Kang Y C and Park S-K 2021 Chemically integrating MXene nanosheets with N-doped C-coated Si nanoparticles for enhanced Li storage performance *Scr. Mater.* **199** 113840

[44] Wang Z, Cao D, Ren M, Zhang H, Pan L, John Zhang C and Yang J 2022 Si@$Ti_3C_2T_x$ with Si nanoparticles embedded in a 3D conductive network of crumpled $Ti_3C_2T_x$ nanosheets for the anode of lithium-ion batteries with enhanced cycling performance *J. Alloys Compd.* **892** 162037

[45] Cao D, Ren M, Xiong J, Pan L, Wang Y, Ji X, Qiu T, Yang J and Zhang C 2020 Self-assembly of hierarchical $Ti_3C_2T_x$-CNT/SiNPs resilient films for high performance lithium ion battery electrodes *Electrochim. Acta* **348** 136211

[46] Hui X, Zhao R, Zhang P, Li C, Wang C and Yin L 2019 Low-temperature reduction strategy synthesized Si/Ti_3C_2 MXene composite anodes for high-performance Li-ion batteries *Adv. Energy Mater.* **9** 1901065

[47] Zhang W, Shi H, Wang D, Wang J, Xiong Z, Wang C, Gu Y, Bai Z, Liang Q and Yan X 2022 Three-dimensional Ti_3C_2 MXene@silicon@nitrogen-doped carbon foam for high performance self-standing lithium-ion battery anodes *J. Electroanal. Chem.* **921** 116664

[48] Peng X, Xiong C, Lin Y, Zhao C and Zhao T 2021 Honeycomb-like hierarchical porous silicon composites with dual protection for ultrastable Li-ion battery anodes *SmartMat* **2** 579–90

[49] Thirumal V, Yuvakkumar R, Kumar P S, Ravi G and Velauthapillai D 2022 Si@MXene/graphene crumbled spherical nanocomposites *Int. J. Energy Res.* **46** 21548–57

[50] Li X, Chen Z, Li A, Yu Y, Chen X and Song H 2020 Three-dimensional hierarchical porous structures constructed by two-stage MXene-wrapped Si nanoparticles for Li-ion batteries *ACS Appl. Mater. Interfaces* **12** 48718–28

[51] Tian Y, An Y and Feng J 2019 Flexible and freestanding silicon/MXene composite papers for high-performance lithium-ion batteries *ACS Appl. Mater. Interfaces* **11** 10004–11

[52] Yan Y, Zhao X, Dou H, Wei J, Sun Z, He Y S, Dong Q, Xu H and Yang X 2020 MXene frameworks promote the growth and stability of LiF-rich solid-electrolyte interphases on silicon nanoparticle bundles *ACS Appl. Mater. Interfaces* **12** 18541–50

[53] Zhou H, Cui C, Cheng R, Yang J and Wang X 2021 MXene enables stable solid-electrolyte interphase for Si@MXene composite with enhanced cycling stability *ChemElectroChem* **8** 3089–94

[54] Al Ja'farawy M S, Hikmah D N, Riyadi U, Purwanto A and Widiyandari H 2021 A review: the development of SiO_2/C anode materials for lithium-ion batteries *J. Electron. Mater.* **50** 6667–87

[55] Zhang K, Zhao D, Qian Z, Gu X, Yang J and Qian Y 2023 N-doped $Ti_3C_2T_x$ MXene sheet-coated SiO_x to boost lithium storage for lithium-ion batteries *Sci. China Mater.* **66** 51–60

[56] Sarang K, Zhao X, Holta D, Cao H, Arole K, Flouda P, Oh E-S, Radovic M, Green M J and Lutkenhaus J L 2021 Carbon additive-free crumpled $Ti_3C_2T_x$ MXene-encapsulated silicon nanoparticle anodes for lithium-ion batteries *ACS Appl. Energy Mater.* **4** 10762–73

[57] Liu S *et al* 2019 Dual bond enhanced multidimensional constructed composite silicon anode for high-performance lithium ion batteries *ACS Nano* **13** 8854–64

[58] Zhang Z, Ying H, Huang P, Zhang S, Zhang Z, Yang T and Han W-Q 2023 Porous Si decorated on MXene as free-standing anodes for lithium-ion batteries with enhanced diffusion properties and mechanical stability *Chem. Eng. J.* **451** 138785

[59] Tang J, Wu F, Dai X, Zhou J, Pang H, Duan X, Xiao B, Li D and Long J 2023 Robust MXene adding enables the stable interface of silicon anodes for high-performance Li-ion batteries *Chem. Eng. J.* **452** 139139

[60] Zhang P, Zhu Q, Guan Z, Zhao Q, Sun N and Xu B 2020 A flexible Si@C electrode with excellent stability employing an MXene as a multifunctional binder for lithium-ion batteries *ChemSusChem* **13** 1621–8

[61] Jiang M, Zhang F, Zhu G, Ma Y, Luo W, Zhou T and Yang J 2020 Interface-amorphized Ti_3C_2@Si/SiO_x@TiO_2 anodes with sandwiched structures and stable lithium storage *ACS Appl. Mater. Interfaces* **12** 24796–805

[62] Nölle R, Beltrop K, Holtstiege F, Kasnatscheew J, Placke T and Winter M 2020 A reality check and tutorial on electrochemical characterization of battery cell materials: how to choose the appropriate cell setup *Mater. Today* **32** 131–46

[63] Wu J *et al* 2019 Recent progress in advanced characterization methods for silicon-based lithium-ion batteries *Small Methods* **3** 1900158

[64] Heubner C, Maletti S, Lohrberg O, Lein T, Liebmann T, Nickol A, Schneider M and Michaelis A 2021 Electrochemical characterization of battery materials in 2-electrode half-cell configuration: a balancing act between simplicity and pitfalls *Batter. Supercaps* **4** 1310–22

[65] Liu Z, Lu D, Wang W, Yue L, Zhu J, Zhao L, Zheng H, Wang J and Li Y 2022 Integrating dually encapsulated Si architecture and dense structural engineering for ultrahigh volumetric and areal capacity of lithium storage *ACS Nano* **16** 4642–53

[66] Wen C J and Huggins R A 1981 Chemical diffusion in intermediate phases in the lithium-silicon system *J. Solid State Chem.* **37** 271–8

[67] Cheng R *et al* 2018 Understanding the lithium storage mechanism of $Ti_3C_2T_x$ MXene *J. Phys. Chem.* C **123** 1099–109

[68] Beaulieu L Y, Eberman K W, Turner R L, Krause L J and Dahn J R 2001 Colossal reversible volume changes in lithium alloys *Electrochem. Solid-State Lett.* **4** A137
[69] Beaulieu L Y, Hatchard T D, Bonakdarpour A, Fleischauer M D and Dahn J R 2003 Reaction of Li with alloy thin films studied by *in situ* AFM *J. Electrochem. Soc.* **150** A1457
[70] Besenhard J O, Yang J and Winter M 1997 Will advanced lithium-alloy anodes have a chance in lithium-ion batteries? *J. Power Sources* **68** 87–90
[71] Chevrier V L, Zwanziger J W and Dahn J R 2010 First principles study of Li–Si crystalline phases: charge transfer, electronic structure, and lattice vibrations *J. Alloys Compd.* **496** 25–36
[72] Hatchard T D and Dahn J R 2004 *In situ* XRD and electrochemical study of the reaction of lithium with amorphous silicon *J. Electrochem. Soc.* **151** A838
[73] Sharma R A and Seefurth R N 1976 Thermodynamic properties of the lithium-silicon system *J. Electrochem. Soc.* **123** 1763
[74] Weydanz W J, Wohlfahrt-Mehrens M and Huggins R A 1999 A room temperature study of the binary lithium–silicon and the ternary lithium–chromium–silicon system for use in rechargeable lithium batteries *J. Power Sources* **81–82** 237–42
[75] Huggins R A 1999 Lithium alloy negative electrodes *J. Power Sources* **81–82** 13–19
[76] Wang X, Hao H, Liu J, Huang T and Yu A 2011 A novel method for preparation of macroposous lithium nickel manganese oxygen as cathode material for lithium ion batteries *Electrochim. Acta* **56** 4065–9
[77] Xu H, Chen G, Du F, Wang X, Dall'Agnese Y and Gao Y 2022 Electrospun $Ti_3C_2T_x$ MXene and silicon embedded in carbon nanofibers for lithium-ion batteries *J. Appl. Phys.* **55** 204002
[78] Wang D, Wang R, Huang K, Lei M and Tang H 2022 Si-P-Ti stabilized Si-P/$Ti_3C_2T_x$ nanohybrids for enhanced lithium-ion storage *Adv. Compos. Hybrid Mater.* **5** 1362–75
[79] Chen G Z 2021 Linear and non-linear pseudocapacitances with or without diffusion control *Prog. Nat. Sci.: Mater. Int.* **31** 792–800
[80] Xiao Z, Lei C, Yu C, Chen X, Zhu Z, Jiang H and Wei F 2020 Si@Si_3N_4@C composite with egg-like structure as high-performance anode material for lithium ion batteries *Energy Storage Mater.* **24** 565–73
[81] Choi C, Ashby D S, Butts D M, DeBlock R H, Wei Q, Lau J and Dunn B 2019 Achieving high energy density and high power density with pseudocapacitive materials *Nat. Rev. Mater.* **5** 5–19
[82] Fleischmann S, Mitchell J B, Wang R, Zhan C, Jiang D E, Presser V and Augustyn V 2020 Pseudocapacitance: from fundamental understanding to high power energy storage materials *Chem. Rev.* **120** 6738–82
[83] Yang Q, Wang Z, Xia Y, Wu G, Chen C, Wang J, Rao P and Dong A 2020 Facile electrostatic assembly of Si@MXene superstructures for enhanced lithium-ion storage *J. Colloid Interface Sci.* **580** 68–76
[84] Mu G, Mu D, Wu B, Ma C, Bi J, Zhang L, Yang H and Wu F 2020 Microsphere-like SiO_2/MXene hybrid material enabling high performance anode for lithium ion batteries *Small* **16** e1905430
[85] Yan Y, He Y-S, Zhao X, Zhao W, Ma Z-F and Yang X 2021 Regulating adhesion of solid-electrolyte interphase to silicon via covalent bonding strategy towards high Coulombic-efficiency anodes *Nano Energy* **84** 105935